Brain network local interconnectivity loss in aging *APOE*-4 allele carriers

Jesse A. Brown[a,b], Kevin H. Terashima[a,b], Alison C. Burggren[a,b], Linda M. Ercoli[b], Karen J. Miller[b], Gary W. Small[b,c], and Susan Y. Bookheimer[a,b,d,1]

[a]Center for Cognitive Neuroscience, Semel Institute for Neuroscience and Human Behavior, [b]Department of Psychiatry and Biobehavioral Sciences, David Geffen School of Medicine, [d]Department of Psychology, and [c]Longevity Center, University of California, Los Angeles, CA 90095

Edited by James L. McGaugh, University of California, Irvine, CA, and approved October 27, 2011 (received for review June 7, 2011)

Old age and possession of the *APOE*-4 allele are the two main risk factors for developing later onset Alzheimer's Disease (AD). Carriers of the *APOE*-4 allele have known differences in intrinsic functional brain network activity across the life span. These individuals also demonstrate specific regional differences in gray and white matter gross structure. However, the relationship of these variations to whole brain structural network connectivity remains unclear. We performed diffusion tensor imaging (DTI), T1 structural imaging, and cognitive testing on aging *APOE*-4 noncarriers (n = 30; mean age = 63.8±8.3) and *APOE*-4 carriers (n = 25; mean age = 60.8 ±9.7). Fiber tractography was used to derive whole brain structural graphs, and graph theory was applied to assess structural network properties. Network communication efficiency was determined for each network by quantifying local interconnectivity, global integration, and the balance between these, the small worldness. Relative to noncarriers, *APOE*-4 carriers demonstrated an accelerated age-related loss of mean local interconnectivity ($r = -0.64$, $P \leq 0.01$) and regional local interconnectivity decreases in the precuneus ($r = -0.64$), medial orbitofrontal cortex ($r = -0.5$), and lateral parietal cortex ($r = -0.54$). *APOE*-4 carriers also showed significant age-related loss in mean cortical thickness ($r = -0.52$, $P < 0.05$). Cognitively, *APOE*-4 carriers had significant negative correlations of age and performance on two episodic memory tasks ($P < 0.05$). This genotype-specific pattern of structural connectivity change with age thus appears related to changes in gross cortical structure and cognition, potentially affecting the rate and/or spatial distribution of AD-related pathology.

complex network | genetics

Although increasing age is the primary risk factor for developing Alzheimer's disease (AD), the disease also has known genetic risk factors. The sole confirmed genetic variant is the apolipoprotein E epsilon 4 allele (*APOE*-4) (1) of which 15–20% of the Caucasian population carries at least one copy. Individuals in this group are three to four times more likely to develop AD and have a younger mean age at onset than *APOE*-4 noncarriers (2). The *APOE* protein functions as the principal cholesterol transporter in the brain and affects diverse cellular processes including development, plasticity, and repair in both gray and white matter (3). Neuroimaging studies of *APOE*-4 carriers and *APOE*-4 noncarriers (*APOE*-4 NCs) have revealed numerous structural and functional brain differences across the life span (4). Whereas *APOE*-4 carriers have been shown to exhibit earlier signs of cognitive decline with aging (5), some genotype-specific brain differences appear before cognitive decline (6–9). *APOE*-4 carriers aged ≥60 y are at elevated risk for developing AD (2) and are thus a critical target for identifying neuroimaging biomarkers of AD risk that accompany cognitive decline associated with disease risk.

Neuronal atrophy is known to follow a characteristic trajectory in AD, originating in temporal, parietal, and limbic cortices and eventually spreading to frontal regions (10). A growing body of recent research has demonstrated that disconnection between regions is a major component of AD, resulting in specific cognitive deficits such as episodic memory loss (11). White matter degradation is concomitant with gray matter loss in AD, typically originating in regions that undergo myelination late in development (12, 13). This loss of axonal myelination reduces the fidelity of communication between brain regions (14), adversely affecting neuronal synchrony (15). This process makes AD and AD genetic risk particularly amenable to study with complex brain network analysis, a methodology for quantifying the brain's communication integration, efficiency, and robustness (16).

Diffusion tensor imaging (DTI) tractography quantifies the density of white matter-insulated axonal bundles that connect different regions of the brain. It is a primary method for characterizing the brain's white matter or "structural" network (17). Structural brain networks inferred from DTI tractography can be reduced to connectivity matrices or "graphs" that describe the strength of connection between any pair of brain regions. These matrices are typically analyzed using graph theory, a branch of mathematics with methods to formally analyze a pattern of connections ("edges") between different entities ("nodes"). Specific regional and global metrics measure the local and global efficiency of information processing by quantifying the density of connections between regions and the distance over which information must transfer (18). Network-based measures of structural and functional brain connectivity can be more sensitive to alterations that are not apparent in gross structure (e.g., cortical thickness or white matter integrity) because they consider each region's integration into the global unit rather than as an independent entity. The brain appears to exhibit small worldness, a balance of two properties: high local clustering, a dense interconnectivity among physically adjacent regions, and high global efficiency, a relatively short distance information must travel between any two nodes in the network (19, 20).

Several independent lines of evidence implicate reduced network connectivity in AD. A recent network-based DTI tractography analysis of AD patients by Lo and colleagues (21) assessed characteristic path length, a measure of the average distance information must transfer between brain regions. In general, a network in which there is a shorter average distance for information to transfer is considered more efficient, given that there is a greater metabolic and structural cost required to

Author contributions: J.A.B., A.C.B., L.M.E., K.J.M., G.W.S., and S.Y.B. designed research; J.A.B., K.H.T., A.C.B., L.M.E., and K.J.M. performed research; J.A.B. and K.H.T. contributed new reagents/analytic tools; J.A.B., K.H.T., A.C.B., L.M.E., and K.J.M. analyzed data; and J.A.B., G.W.S., and S.Y.B. wrote the paper.

Conflict of interest statement: The authors declare a conflict of interest. G.W.S. reports having served as a consultant and/or having received lecture fees from Dakim, Eisai, Forest, Medivation, Novartis, and Pfizer. G.W.S. also reports having received stock options from Dakim.

This article is a PNAS Direct Submission.

Data deposition: The connectivity matrices for each subject in this study have been uploaded to the University of California, Los Angeles (UCLA) Multimodal Connectivity Database, http://umcd.ccn.ucla.edu, where they are publicly available.

[1]To whom correspondence should be addressed. E-mail: sbook@ucla.edu.

This article contains supporting information online at www.pnas.org/lookup/suppl/doi:10.1073/pnas.1109038108/-/DCSupplemental.

transmit information over a longer distance. Lo et al. found that AD patients had significantly higher characteristic path length than control individuals, indicating reduced global efficiency. Resting state fMRI connectivity studies of AD patients have also consistently revealed network deficits. Reduced functional connectivity in the brain's default mode network (DMN) is a hallmark of AD (22). This network is composed of the posterior cingulate, medial prefrontal cortex, lateral inferior parietal cortex, lateral inferior temporal cortex, anterior cingulate, medial temporal lobe, and precuneus (23, 24). The DMN is highly metabolically active, particularly when an individual has internally focused attention, such as during episodic memory retrieval (25, 26). Importantly, DMN hubs in the posterior cingulate, precuneus, and medial prefrontal cortex have also been shown to exhibit a striking overlap with the sites of greatest Aβ deposition in AD (27).

In cognitively normal *APOE*-4 carriers, structural brain connectivity has primarily been assessed by looking at gross measures of white matter integrity such as fractional anisotropy (FA) and apparent diffusion coefficient (ADC). In older *APOE*-4 carriers, age-related decreases in myelination (28) and FA (29) have been observed that are more rapid than those in noncarriers, particularly in the frontal and temporal lobes. There is also substantial evidence that older *APOE*-4 carriers perform worse than noncarriers on episodic memory tests (30). It remains unclear which structural and functional brain changes drive these declines in cognitive performance.

Here we used DTI and a hybrid probabilistic/deterministic tractography approach to characterize fiber network topology in aging subjects with genetic risk for AD. We analyzed the fiber networks of *APOE*-4 noncarriers and *APOE*-4 carriers for path length, clustering, and small worldness to assess local and global variations in network topology that may be associated with cognitive decline and precede the conversion to AD.

Results

Cognitive Performance. Cognitive scores on all neuropsychological tests were compared for *APOE*-4 carriers and noncarriers, using two-sample two-tailed *t* tests (Table 1). No significant between-group differences were found with the exception of the mini-mental state examination (MMSE). However, when MMSE was included as a covariate in subsequent statistical analyses, it did not affect any statistical results. Relationships between age and cognitive performance were tested in two ways. First, within genotype group, partial correlations were calculated between age and each neuropsychological measure, controlling for sex, years of education, and family history of dementia. Second, a stepwise regression was run, starting with a model of *APOE* status (carrier or noncarrier), sex, age, and *APOE* × age interaction. In all cases reported here, the model with *APOE* status, sex, and *APOE* × age interaction yielded the most accurate predictions (*Methods*). *APOE*-4 carriers exhibited significant negative partial correlations with age on the Rey–Osterrith Complex Figure (ROF), delayed recall (delay ROF; $r = -0.57$, $P = 0.005$), and Wechsler memory scale (WMS), logical memory (LM) delayed recall portion (delay total LM; $r = -0.44$, $P = 0.04$) (Fig. S1). *APOE*-4 noncarriers had no significant age-related reduction in score on these tests. The partial correlation values were significantly different for Rey–Osterrith (Rey-O) delay ($P = 0.01$) and there was a trend toward difference for the WMS LM delay ($P = 0.08$). The regression model found the *APOE* × age interaction to be significant for both the delay total LM ($P = 0.02$) and delay ROF ($P = 0.001$) tests.

Age Effects on Global Network Connectivity. Structural connectivity matrices were analyzed for each subject to determine global structural network measures of global integration (characteristic path length), local interconnectivity (mean clustering coefficient), the balance of integration and interconnectivity (small worldness), and the total amount of fiber constituting the network (total network cost). These metrics were then assessed for genotype-specific age-related changes. The partial correlation was calculated between all structural network metrics and age, controlling for sex, scanner, and total network cost. The inclusion of total network cost ensured that differences in clustering coefficient between *APOE*-4 carriers and *APOE*-4 noncarriers were not driven by differences in the total amount of axonal fibers between groups. The partial correlation of clustering coefficient and age was strongly negative for *APOE*-4 carriers ($r = -0.64$, $P = 0.002$) and nonsignificant for *APOE*-4 noncarriers ($r = -0.21$ $P = 0.28$) (Fig. 1*A*). These partial correlation values were significantly different ($P = 0.03$) and the regression model found that the *APOE* × age interaction was significant ($P = 0.0005$).

The partial correlation between characteristic path length and age trended toward significance for *APOE*-4 noncarriers ($r = 0.36$, $P = 0.08$) but was nonsignificant for *APOE*-4 carriers ($r = 0.21$, $P = 0.37$). The correlation values were not significantly different and the regression found no significant *APOE* × age interaction for characteristic path length.

To look at the combined effect of clustering coefficient and characteristic path length, small worldness (σ) was assessed separately for the two groups. *APOE*-4 carriers exhibited a strong negative correlation between age and small worldness ($r = -0.52$,

Table 1. Subject characteristics

Characteristic (mean ± SD)	*APOE*-4 NC	*APOE*-4	*P*	*APOE*-4 NC partial correlation with age	*APOE*-4 partial correlation with age
Age, y	63.8 ± 8.3	60.8 ± 9.7	0.22		
Age range	45–76	43–78			
No. (males/females)	30 (10/20)	25 (12/13)			
Education, y	16.7 ± 1.8	17.5 ± 3.3	0.33		
Family history, yes/no	21/9	16/9			
MMSE, score range 0–30	29.4 ± 0.9	28.6 ± 1.2	0.01*	$r = -0.41$, $P = 0.07$	$r = -0.14$, $P = 0.55$
WMS LM delay, 0–50	29.1 ± 7.1	27.1 ± 9.2	0.45	$r = -0.09$, $P = 0.66$	$r = -0.45$, $P = 0.038$*
Buschke CLTR, 0–144	56.7 ± 39.7	57.8 ± 34.2	0.92	$r = -0.16$, $P = 0.44$	$r = -0.36$, $P = 0.1$
Rey-O delay, 0–36	12.9 ± 7.2	13.8 ± 7.1	0.68	$r = -0.03$, $P = 0.87$	$r = -0.57$, $P = 0.005$*
WMS VP, 0–32	22.3 ± 7.4	20.6 ± 8.2	0.49	$r = -0.17$, $P = 0.38$	$r = 0.05$, $P = 0.8$
WAIS digit span	17.7 ± 3.6	18.1 ± 3.1	0.65	$r = 0.21$, $P = 0.29$	$r = 0.1$, $P = 0.65$

Partial correlations with age were controlled for sex, years of education, and family history of dementia. Buschke CLTR, Buschke–Fuld selective reminding test, consistent long-term retrieval section; MMSE, mini-mental state examination; NC, noncarriers; Rey-O delay, Rey–Osterrith Complex Figure, delayed recall; WAIS digit span, Wechsler Adult Intelligence Scale 3, digit span; WMS LM delay, Wechsler memory scale, logical memory delayed recall portion; WMS VP, Wechsler memory scale, verbal paired associations II. *$P < 0.05$.

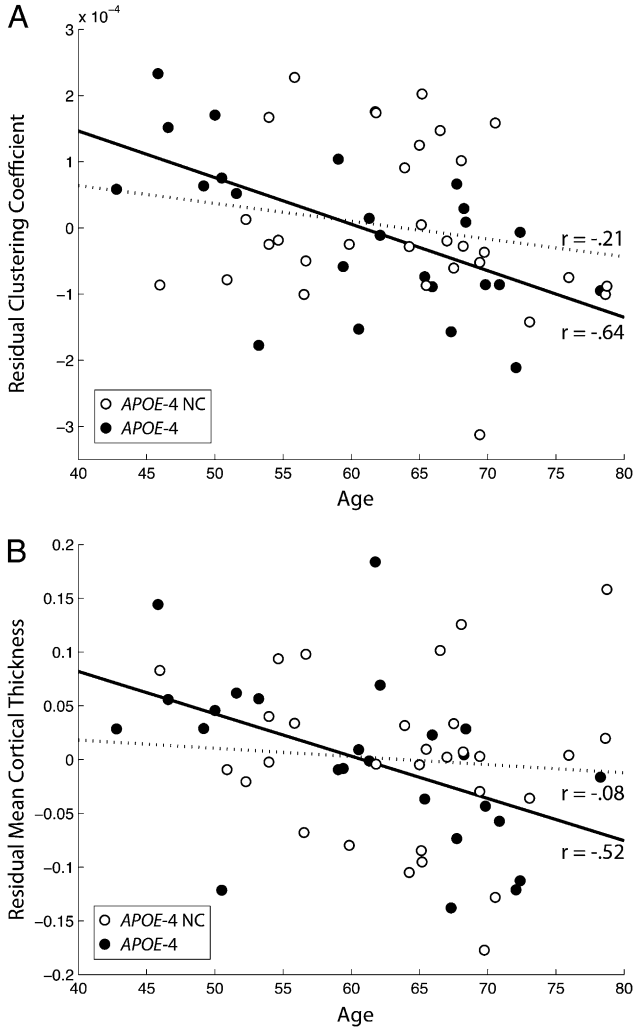

Fig. 1. (*A* and *B*) Mean clustering coefficient (MCC) and mean cortical thickness (MCT) residuals based on partial correlations with age plotted for *APOE*-4 noncarriers (*APOE*-4 NC, open circles, dashed line) and *APOE*-4 carriers (solid circles, solid line). Partial correlations controlled for sex, scanner, and, in the MCC case only, total network cost. Both MCC and MCT had a significant interaction between *APOE* and genotype ($P < 0.05$).

$P = 0.01$) whereas *APOE*-4 noncarriers showed no significant relationship ($r = -0.26$, $P = 0.2$). However, partial correlation coefficients did not significantly differ and regression did not find a significant *APOE* × age interaction for small worldness.

Finally, measurements of total network cost were compared with age. The partial correlation of age and total cost was significantly negative for *APOE*-4 carriers ($r = -0.44$, $P = 0.02$) but not for *APOE*-4 noncarriers ($r = -0.31$, $P = 0.18$). However, partial correlation coefficients were not significantly different, and regression did not find a significant *APOE* × age interaction.

Age Effects on Regional Network Connectivity. We next examined whether the relationship between age and network characteristics varied by region for *APOE*-4 carriers and noncarriers. The analysis was focused on regional clustering coefficients because mean clustering coefficients showed a global *APOE* × age interaction effect. For the model to best predict a regional clustering coefficient, the set of terms that stepwise regression found to best fit the mean clustering coefficient was used. This model included *APOE*, sex, *APOE* × age interaction, total cost, and scanner. At a false discovery rate (FDR)-corrected α of $P = 0.05$, several regions showed a significant interaction where *APOE*-4 carriers decreased more sharply than noncarriers: the right precuneus ($P = 0.00006$), left orbitofrontal cortex ($P = 0.004$), left supramarginal gyrus ($P = 0.002$), and right inferior temporal gyrus anteriorly ($P = 0.0009$) and posteriorly ($P = 0.002$) (Fig. 2). At an exploratory threshold of $P < 0.005$ (uncorrected), additional regions displaying a potential *APOE* × age interaction included right subcallosal cortex (part of the ventromedial prefrontal cortex, $P = 0.009$) and right precentral gyrus ($P = 0.009$) (Fig. 2). These regions all showed significant negative partial correlations with age for *APOE*-4 carriers, no significant correlation for *APOE*-4 noncarriers, and a significant difference in correlation coefficients ($P < 0.05$) (Table S2).

Cortical Thickness. The mean cortical thickness values were also examined in relationship to age for *APOE*-4 carriers and noncarriers. *APOE*-4 carriers demonstrated a significant negative partial correlation between cortical thickness and age ($r = -0.52$, $P = 0.01$) whereas noncarriers displayed no relationship ($r = -0.09$, $P = 0.66$) (Fig. 1*B*). The partial correlation coefficients were significantly different ($P = 0.047$) and regression found a significant *APOE* × age interaction for cortical thickness ($P = 0.003$).

Finally, the relationship between mean cortical thickness and mean clustering coefficient was tested by examining the within-genotype partial correlation of the two measures, controlling for the effects of scanner and total cost. The relationship was strongly positive for *APOE*-4 carriers ($r = 0.64$, $P = 0.001$) but showed no significant trend for noncarriers ($r = 0.04$, $P = 0.84$). These partial correlation coefficients were significantly different ($P = 0.02$).

Discussion

This study of axonal fiber networks found that aging *APOE*-4 carriers showed a significantly more negative relationship between local interconnectivity and age than noncarriers. *APOE*-4 carriers also exhibited a significant decrease in small worldness with age, although no significant interaction between *APOE* and age was detected. Neither *APOE*-4 carriers nor noncarriers showed significant relationships between characteristic path length and age, indicating no major loss of global structural integration. Small worldness represents the balance of clustering coefficient (local interconnectivity) and characteristic path length (global integration) in a real network with respect to a random network. Here it appears that the *APOE*-4 carrier age-related reduction in small worldness was driven primarily by the loss of local interconnectivity whereas global integration was relatively spared.

APOE-4 carriers also showed a significant negative relationship of cortical thickness with age. This decrease paralleled the reduction in structural network local interconnectivity with age, suggesting a relationship between cortical thickness and the degree of local structural connectivity. This relationship was explicitly tested by calculating the partial correlation of mean cortical thickness and mean clustering coefficient for each genotype group. This relationship was significantly more positive for *APOE*-4 carriers. It is possible that the relationship between these two measures grows stronger as they decrease, which would help explain why only *APOE*-4 carriers showed this association. Alternatively, the *APOE*-4 allele may contribute to a tighter relationship between these brain structural properties. The finding of cortical thinning with age in *APOE*-4 carriers is not without precedence, as a previous report (31) found that aging *APOE*-4 carriers have (*i*) higher cortical thickness when controlling for age and (*ii*) a stronger age-related decrease in cortical thickness than noncarriers. However, it should be noted that in the current study the relationship of local interconnectivity and age was more pronounced than the decrease in cortical thickness, indicating

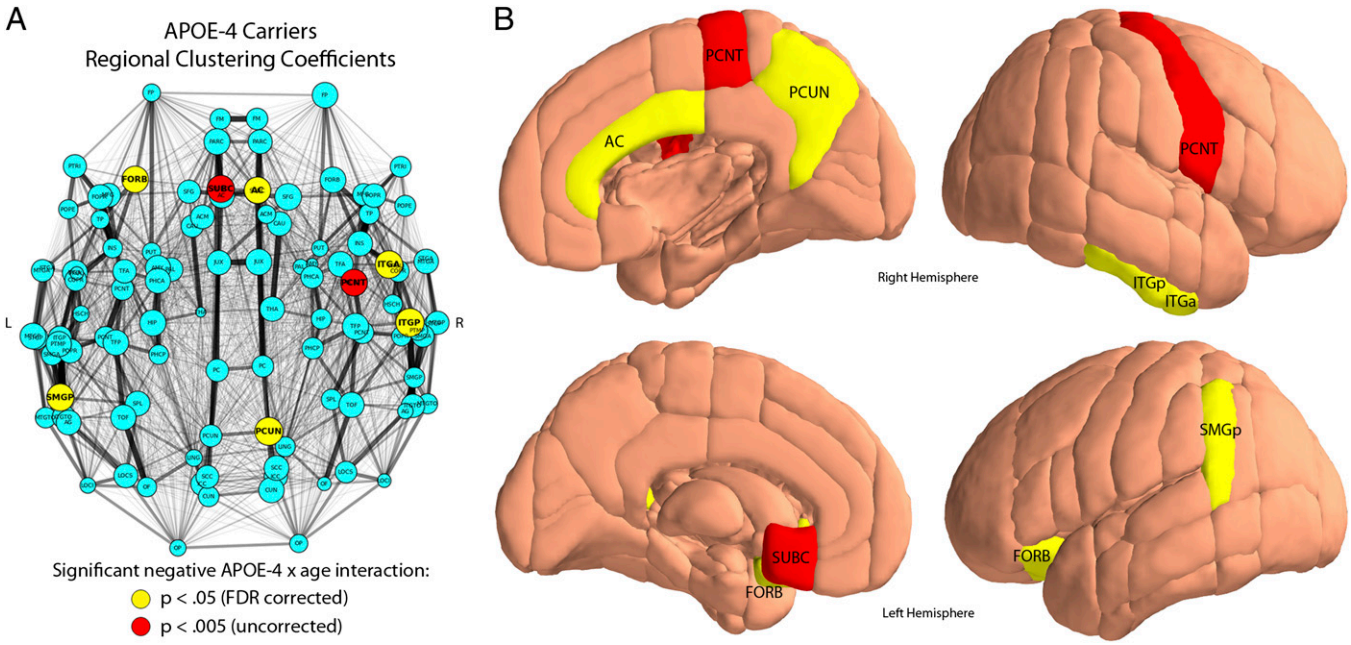

Fig. 2. (*A*) DTI average weighted network with node radius corresponding to value of negative correlation of age with clustering coefficient for *APOE*-4 carriers. The width of each edge in the graph corresponds to the average fiber density between those regions. Nodes colored in yellow have significant negative *APOE*-4 × age interactions for clustering coefficient ($P < 0.05$, FDR corrected), nodes colored in red indicate the same measure at an exploratory threshold ($P < 0.005$, uncorrected). (*B*) The same nodes from *A* displayed on an anatomical brain model. Node abbreviations: AC, anterior cingulate; FORB, frontal orbital cortex; ITGa, inferior temporal gyrus (anterior); ITGp, inferior temporal gyrus; PCNT, precentral gyrus; PCUN, precuneus (posterior); SMGp, supramarginal gyrus (posterior); and SUBC, subcallosal cortex (part of the ventromedial prefrontal cortex).

partial independence of these measures and the utility of both in detecting age-related changes that may precede the conversion to AD.

The age-related reduction in local interconnectivity among *APOE*-4 carriers in this study appeared to be especially driven by the younger subjects, who had the highest measurements of clustering coefficient. The relationship between high structural local connectivity and brain health in general is not entirely clear. The first study of DTI structural network properties and intelligence found a positive relationship between intelligence quotient and clustering coefficient (32). The *APOE*-4 carriers in the present study had significant negative relationships of performance and age on two different episodic memory tasks, supporting the notion that decreasing interconnectivity has negative cognitive consequences. Importantly, previous evidence does suggest higher connectivity in young *APOE*-4 carriers. A study of resting state fMRI patterns found healthy *APOE*-4 carriers in young adulthood exhibited greater DMN connectivity than noncarriers (33). Similar studies in older *APOE*-4 carriers have shown a complex pattern of increased and decreased functional connectivity with respect to noncarriers (34, 35). Overall, there appears to be a unique age-related trajectory of connectivity change across the life span for *APOE*-4 carriers. Specifically, there is an apparent higher degree of connectivity early in life that declines more steeply across the age span. Interestingly, a similar pattern appears to hold for cognitive abilities associated with *APOE*-4. Several cognitive studies in healthy *APOE*-4 carriers and noncarriers have found better cognitive performance for young *APOE*-4 carriers (36, 37), a trend that reverses for *APOE*-4 carriers in their 50s with declines in memory occurring the earliest (38). This developmental trajectory has been hypothesized as a case of antagonistic pleiotropy, in which the *APOE*-4 allele offers benefits during development and early adulthood at the expense of more rapid decline with aging (30). Alternatively, local connectivity has been shown to reduce during development in the years when pruning is the dominant structural process (39, 40), which may indicate that *APOE*-4 carriers undergo less pruning. Regardless of the potential benefit that higher local interconnectivity may provide, it is tempting to speculate that *APOE*-4 carrier-specific increases in metabolic activity within the default mode network may reflect higher structural local connectivity. Elevated metabolic activity could conceivably contribute to increased amyloid production and aggregation over time (27, 41). Although the underlying causes of these different developmental trajectories are currently unknown, it is clear that the *APOE*-4 allele does not simply cause reduced anatomical connectivity and cognitive performance across the life span (42). Future structural network studies in developing and young individuals should shed light on the possibility of increased local interconnectivity in *APOE*-4 carriers.

Many regions that are part of the default mode network showed a negative correlation between age and local interconnectivity for *APOE*-4 carriers in this study; specifically, the right precuneus, left inferior parietal lobule (supramarginal gyrus), ventromedial and orbital prefrontal cortex, and anterior cingulate gyrus have all been cited as components of the DMN (24, 43, 44) although there is some heterogeneity in the precise definition of the DMN. The majority of the regions that exhibited significant negative correlations of age and clustering are connected to one another. Because clustering coefficient is a measure of connectivity among a region's first-degree neighbors, the implication is that there is less total connectivity within this network of regions with aging in *APOE*-4 carriers. These findings are consistent with prior studies showing decreased resting fMRI correlation between the medial prefrontal cortex, lateral parietal cortex, and posterior cingulate in older individuals harboring high amyloid burden (45). In older individuals with subjective memory complaints, amyloid levels have also been associated with cortical thinning of the medial orbital frontal cortex, anterior cingulate, and precuneus (46). In the current study, the combined impact of aging and genetic risk contributes to lower connectivity and cortical thickness within the

DMN and other structural hubs as age increases. Furthermore, this decreased interconnectivity appears to have behavioral consequences, as *APOE*-4 carriers exhibited significant age-related reduction in episodic memory performance. This DMN-memory relationship is consistent with the putative role of the DMN in episodic memory retrieval (26) and suggests a potential link between anatomical and behavioral phenotypes.

The use of DTI to construct a whole brain fiber network has known limitations. DTI is not ideal for detecting crossing fibers. However, we used a hybrid probabilistic–deterministic tractography method to improve sensitivity to the detection of crossing fibers. Furthermore, network hubs were observed in expected regions including the precuneus, posterior cingulate, and insula (Table S2). Because four of the *APOE*-4 carriers were 4/4 homozygotes, local interconnectivity, cortical thickness, and two episodic memory tests showing negative correlation with age (WMS LM delay and Rey-O delay) were tested in the same regression model after excluding the four homozygotes. All properites remained significantly negatively related to age. This result indicates no significant additive effect of an additional e4 allele.

In this study we examined axonal fiber networks in healthy aging *APOE*-4 carriers and noncarriers and found *APOE*-4 carriers exhibited a negative correlation of local structural connectivity with age that was tightly coupled to reductions in cortical thickness. Additionally, they demonstrated accelerated decrease of small worldness with age, suggesting a more rapid loss in the balance between global integration and local modularity of information processing. At the regional level, *APOE*-4 carriers were found to have age-related loss of interconnectivity among regions composing the default mode network. *APOE*-4 carriers also demonstrated significant decreases in performance with age on two different episodic memory tasks that are known to engage the affected regions. Genetic variations in the structure and function of these networks may contribute to differential rates of amyloid production with age and eventual impairment of brain communication efficiency.

Methods

Subject Inclusion and Imaging. Fifty-five subjects participated in this study. Subjects are summarized in Table 1 with additional details in *SI Methods*. Any subject who possessed at least one *APOE*-4 allele was categorized as an "*APOE*-4 carrier"; subjects homozygous for the *APOE*-3 allele were designated as "noncarriers" or equivalently, "*APOE*-4 noncarriers." All e2 carriers were excluded. All subjects in these groups were without dementia, based on (*i*) MMSE score ≥26; (*ii*) a composite neuropsychological test score including immediate memory, delayed memory, and nonmemory components; and (*iii*) subjective memory scores from the Memory Functioning Questionnaire (47) (Table 1). All subjects collectively scored within 1 SD of the age-adjusted average on the tests listed in Table 1.

All subjects received T1 structural and 30-direction DTI scans. Forty subjects were scanned on a 3T Siemens Allegra and 25 subjects were scanned on a Siemens 3T Trio. DTI was run with single-shot echo-planar sequences with the following parameters (Trio differences in parentheses): 30 diffusion weighted volumes with gradient vectors taken from the International Consortium for Brain Mapping protocol (48), 5 B0 volumes (1 B0), $b = 800$ s/mm^2 (1,000 s/mm^2), axial slicing, repetition time (TR) = 7,300 ms (7,000 ms), echo time (TE) = 95 ms (86 ms), *k*-space matrix = 96 × 96, slice thickness = 2.5 mm, 55 slices with no gap, field of view = 240 mm^2, and voxel size = 2.5 mm^3. Subjects also received T1-weighted magnetization-prepared rapid gradient echo (MP-RAGE) scans with the following parameters: sagittal slicing, TR = 2,300 ms (1,900 ms), TE = 2.93 ms (2.26 ms), matrix = 192 × 192 (256 × 224), 160 slices with no gap (176), field of view = 256 mm^2 (218 × 250 mm), flip angle = 8° (9°), and voxel size = 1 mm^3. To control for scanner-specific differences, scanner was included as a dummy covariate in all subsequent statistical analyses.

DTI Processing and Tractography. DTI tractography was performed using the first and second dyad vectors calculated by FMRIB Software Library (FSL)'s BEDPOSTX program as the input to Diffusion Toolkit's (http://trackvis.org/dtk) fiber assignment by continuous tracking (FACT) algorithm (*SI Methods*) (49). To obtain each subject's connectivity matrix, the brain was partitioned into 110 regions using the Harvard–Oxford subcortical and cortical probabilistic atlases distributed with FSL. Regions included 7 subcortical regions from each hemisphere (excluding the midbrain) and 47 cortical regions from each hemisphere. Next, the set of fibers connecting each pair of regions was counted to derive a 110 × 110 whole brain connectivity matrix, using custom software written for this purpose [University of California (Los Angeles) Multimodal Connectivity Package, http://www.ccn.ucla.edu/wiki/index.php/UCLA_Multimodal_Connectivity_Package].

Network Construction and Analysis. Fiber density matrices were obtained by scaling the raw fiber count between region–region pairs by the summed volume of the two regions, to control for the unequal number of voxels in each region (*SI Methods*). We sought to compare subject networks at their intrinsic densities rather than artificially removing connections to force equivalent density (50) and therefore did not perform thresholding. To control for individual differences in density, total network cost was included as a covariate in all statistical analyses. To account for the white matter "fidelity", each connection weight was scaled by the averaged FA for all fibers composing that connection.

Network metrics for each subject were quantified using the Brain Connectivity Toolbox (http://sites.google.com/a/brain-connectivity-toolbox.net/bct/metrics). All analyses used weighted networks to calculate the node strengths, clustering coefficients, characteristic path lengths, betweenness centrality, and small worldness. The formulas used to quantify all metrics are described in detail elsewhere (16) and implementations of these from the Brain Connectivity Toolbox were used (*SI Methods*).

Cortical Thickness. Cortical thickness values were obtained on the basis of the analysis of the MP-RAGE scans, using the Freesurfer package (http://surfer.nmr.mgh.harvard.edu) (51). Specifically, the recon-all program was used to normalize image intensities, skull strip, and automatically delineate the white matter and pial (gray matter) surfaces on the basis of the use of intensity gradients to optimally place the borders between tissue types. The distance between the surfaces was measured for ∼220,000 vertex pairs per subject. The average of these thickness measures was used as the measurement of mean cortical thickness for each subject.

Statistical Analysis. All age-related analyses calculated Pearson's partial correlation coefficient (and the associated *P* value) between age and the global/regional network metric of interest, separately for *APOE*-4 carriers and noncarriers, after controlling for the effects of sex, scanner, and total network cost for structural network metrics. To assess between-group differences, we tested three statistical models for each cognitive and global neuroimaging measure. For all models of scanning-related measures, a dummy covariate for scanner (Allegra/Trio) was included. For all models of structural network metrics, a total network cost covariate was included to account for the individual differences in fiber volume.

The first model included only main effects of genotype, sex, and age. The second model added a genotype × age interaction to the model. The third model (model 3) was selected by a stepwise regression procedure that returned the subset of terms producing the most accurate linear regression model. This model began with genotype, sex, age, and genotype × age interaction. In the case of the Rey-O delay, WMS LM delay, cortical thickness, and mean clustering coefficient, the model unanimously offering the best predictions included genotype, sex, and the genotype × age interaction. The interpretability of this model was confirmed by performing a partial correlation of age and each measure, separately for the age-matched *APOE*-4 carriers and noncarriers, controlling for sex (and scanner/total network cost where appropriate). In each case, the correlation coefficient was significantly negative for *APOE*-4 carriers but not for noncarriers ($P < 0.05$) (Table 1 and *Results*). Model 3 was therefore used to examine the interactive effect of genotype and age on regional clustering coefficients. For all regions demonstrating a significant genotype × age interaction, the partial correlation of age and regional clustering was significantly negative for the *APOE*-4 carriers and significantly different from that of the noncarriers ($P < 0.05$) (Table S2). The overall *F* statistics for all three models are shown in *SI Methods*. For all models, we tested the effect of including covariates for years of education and family history of dementia. These variables never exhibited any significant main effect on any of the results and were excluded from the models reported on here to maximize degrees of freedom.

For behavioral measures and global network measures, a *P* value of 0.05 was used to determine significant difference/correlation. For regional network measures, the *P* values for a given measure were adjusted to correct for multiple comparisons, using a FDR procedure with a *q* value of 0.05. In all cases examining age relationships, one-tailed tests of *P* values were

performed, focusing solely on significant negative *APOE*-4 × age interactions. The focus on negative relationships was based on the substantial body of prior findings in similar populations in the literature indicating that aging *APOE*-4 carriers exhibit faster rates of decline in cortical thickness (31), 1 − (apparent diffusion coefficient) (29), and memory scores (38). Consequently, we did not test effects that may increase with age. Regional network measures were predicted with a robust regression model that downweighted outlying observations.

ACKNOWLEDGMENTS. We thank Mike Jones and Brian Renner for data collection. Jeff Rudie provided valuable review of the manuscript. This work was supported by National Institutes of Health National Research Service Award 1F31AG035438-01 (to J.A.B.); by National Institutes of Health Grants P01-AG025831, AG13308, P50 AG 16570, MH/AG58156, MH52453, AG10123, and M01-RR00865; by the Department of Energy (Contract DE-FC03-87-ER60615); by the General Clinical Research Centers Program; by the Fran and Ray Stark Foundation Fund for Alzheimer's Disease Research; and by the Ahmanson Foundation.

1. Naj AC, et al. (2011) Common variants at MS4A4/MS4A6E, CD2AP, CD33 and EPHA1 are associated with late-onset Alzheimer's disease. *Nat Genet* 43:436–441.
2. Corder EH, et al. (1993) Gene dose of apolipoprotein E type 4 allele and the risk of Alzheimer's disease in late onset families. *Science* 261:921–923.
3. Mahley RW (1988) Apolipoprotein E: Cholesterol transport protein with expanding role in cell biology. *Science* 240:622–630.
4. Bookheimer S, Burggren A (2009) *APOE*-4 genotype and neurophysiological vulnerability to Alzheimer's and cognitive aging. *Annu Rev Clin Psychol* 5:343–362.
5. Caselli RJ, et al. (2004) Longitudinal changes in cognition and behavior in asymptomatic carriers of the *APOE* e4 allele. *Neurology* 62:1990–1995.
6. Reiman EM, et al. (2005) Correlations between apolipoprotein E ε4 gene dose and brain-imaging measurements of regional hypometabolism. *Proc Natl Acad Sci USA* 102:8299–8302.
7. Small GW, et al. (2000) Cerebral metabolic and cognitive decline in persons at genetic risk for Alzheimer's disease. *Proc Natl Acad Sci USA* 97:6037–6042.
8. Small GW, et al. (2009) Influence of cognitive status, age, and *APOE*-4 genetic risk on brain FDDNP positron-emission tomography imaging in persons without dementia. *Arch Gen Psychiatry* 66:81–87.
9. Bookheimer SY, et al. (2000) Patterns of brain activation in people at risk for Alzheimer's disease. *N Engl J Med* 343:450–456.
10. Thompson PM, et al. (2003) Dynamics of gray matter loss in Alzheimer's disease. *J Neurosci* 23:994–1005.
11. Delbeuck X, Van der Linden M, Collette F (2003) Alzheimer's disease as a disconnection syndrome? *Neuropsychol Rev* 13:79–92.
12. Stricker NH, et al. (2009) Decreased white matter integrity in late-myelinating fiber pathways in Alzheimer's disease supports retrogenesis. *Neuroimage* 45:10–16.
13. Salat DH, et al. (2010) White matter pathology isolates the hippocampal formation in Alzheimer's disease. *Neurobiol Aging* 31:244–256.
14. Bartzokis G, Lu PH, Mintz J (2007) Human brain myelination and amyloid beta deposition in Alzheimer's disease. *Alzheimers Dement* 3:122–125.
15. Stam CJ, Jones BF, Nolte G, Breakspear M, Scheltens P (2007) Small-world networks and functional connectivity in Alzheimer's disease. *Cereb Cortex* 17:92–99.
16. Rubinov M, Sporns O (2010) Complex network measures of brain connectivity: Uses and interpretations. *Neuroimage* 52:1059–1069.
17. Hagmann P, et al. (2008) Mapping the structural core of human cerebral cortex. *PLoS Biol* 6:e159.
18. Bullmore E, Sporns O (2009) Complex brain networks: Graph theoretical analysis of structural and functional systems. *Nat Rev Neurosci* 10:186–198.
19. Iturria-Medina Y, Sotero RC, Canales-Rodríguez EJ, Alemán-Gómez Y, Melie-García L (2008) Studying the human brain anatomical network via diffusion-weighted MRI and Graph Theory. *Neuroimage* 40:1064–1076.
20. Achard S, Bullmore E (2007) Efficiency and cost of economical brain functional networks. *PLoS Comput Biol* 3:e17.
21. Lo C-Y, et al. (2010) Diffusion tensor tractography reveals abnormal topological organization in structural cortical networks in Alzheimer's disease. *J Neurosci* 30: 16876–16885.
22. Greicius MD, Srivastava G, Reiss AL, Menon V (2004) Default-mode network activity distinguishes Alzheimer's disease from healthy aging: Evidence from functional MRI. *Proc Natl Acad Sci USA* 101:4637–4642.
23. Margulies DS, et al. (2009) Precuneus shares intrinsic functional architecture in humans and monkeys. *Proc Natl Acad Sci USA* 106:20069–20074.
24. Mevel K, Chételat G, Eustache F, Desgranges B (2011) The default mode network in healthy aging and Alzheimer's disease. *Int J Alzheimers Dis* 2011:535816.
25. Raichle ME, et al. (2001) A default mode of brain function. *Proc Natl Acad Sci USA* 98: 676–682.
26. Kim H, Daselaar SM, Cabeza R (2010) Overlapping brain activity between episodic memory encoding and retrieval: Roles of the task-positive and task-negative networks. *Neuroimage* 49:1045–1054.
27. Buckner RL, et al. (2009) Cortical hubs revealed by intrinsic functional connectivity: Mapping, assessment of stability, and relation to Alzheimer's disease. *J Neurosci* 29: 1860–1873.
28. Bartzokis G, et al. (2006) Apolipoprotein E genotype and age-related myelin breakdown in healthy individuals: Implications for cognitive decline and dementia. *Arch Gen Psychiatry* 63:63–72.
29. Ryan L, et al. (2011) Age-related differences in white matter integrity and cognitive function are related to *APOE* status. *Neuroimage* 54:1565–1577.
30. Tuminello ER, Han SD (2011) The apolipoprotein e antagonistic pleiotropy hypothesis: Review and recommendations. *Int J Alzheimers Dis* 2011:726197.
31. Espeseth T, et al. (2008) Accelerated age-related cortical thinning in healthy carriers of apolipoprotein E epsilon 4. *Neurobiol Aging* 29:329–340.
32. Li Y, et al. (2009) Brain anatomical network and intelligence. *PLoS Comput Biol* 5: e1000395.
33. Filippini N, et al. (2009) Distinct patterns of brain activity in young carriers of the *APOE*-ε4 allele. *Proc Natl Acad Sci USA* 106:7209–7214.
34. Fleisher AS, et al. (2009) Resting-state BOLD networks versus task-associated functional MRI for distinguishing Alzheimer's disease risk groups. *Neuroimage* 47: 1678–1690.
35. Sheline YI, et al. (2010) *APOE4* allele disrupts resting state fMRI connectivity in the absence of amyloid plaques or decreased CSF Aβ42. *J Neurosci* 30:17035–17040.
36. Mondadori CRA, et al. (2007) Better memory and neural efficiency in young apolipoprotein E ε4 carriers. *Cereb Cortex* 17:1934–1947.
37. Han SD, et al. (2007) Apolipoprotein E and traumatic brain injury in a military population: Evidence of a neuropsychological compensatory mechanism? *J Neurol Neurosurg Psychiatry* 78:1103–1108.
38. Caselli RJ, et al. (2009) Longitudinal modeling of age-related memory decline and the *APOE* epsilon4 effect. *N Engl J Med* 361:255–263.
39. Hagmann P, et al. (2010) White matter maturation reshapes structural connectivity in the late developing human brain. *Proc Natl Acad Sci USA* 107:19067–19072.
40. Luo L, O'Leary DDM (2005) Axon retraction and degeneration in development and disease. *Annu Rev Neurosci* 28:127–156.
41. Bero AW, et al. (2011) Neuronal activity regulates the regional vulnerability to amyloid-β deposition. *Nat Neurosci* 14:750–756.
42. Han SD, Bondi MW (2008) Revision of the apolipoprotein E compensatory mechanism recruitment hypothesis. *Alzheimers Dement* 4:251–254.
43. Greicius MD, Krasnow B, Reiss AL, Menon V (2003) Functional connectivity in the resting brain: A network analysis of the default mode hypothesis. *Proc Natl Acad Sci USA* 100:253–258.
44. Andrews-Hanna JR, Reidler JS, Sepulcre J, Poulin R, Buckner RL (2010) Functional-anatomic fractionation of the brain's default network. *Neuron* 65:550–562.
45. Hedden T, et al. (2009) Disruption of functional connectivity in clinically normal older adults harboring amyloid burden. *J Neurosci* 29:12686–12694.
46. Chételat G, et al.; Australian Imaging Biomarkers and Lifestyle Research Group (2010) Relationship between atrophy and beta-amyloid deposition in Alzheimer disease. *Ann Neurol* 67:317–324.
47. Gilewski MJ, Zelinski EM, Schaie KW (1990) The Memory Functioning Questionnaire for assessment of memory complaints in adulthood and old age. *Psychol Aging* 5: 482–490.
48. Jones DK, Horsfield MA, Simmons A (1999) Optimal strategies for measuring diffusion in anisotropic systems by magnetic resonance imaging. *Magn Reson Med* 42:515–525.
49. Mori S, van Zijl PCM (2002) Fiber tracking: Principles and strategies - a technical review. *NMR Biomed* 15:468–480.
50. Zalesky A, et al. (2010) Whole-brain anatomical networks: Does the choice of nodes matter? *Neuroimage* 50:970–983.
51. Fischl B, Dale AM (2000) Measuring the thickness of the human cerebral cortex from magnetic resonance images. *Proc Natl Acad Sci USA* 97:11050–11055.

Supporting Information

Brown et al. 10.1073/pnas.1109038108

SI Methods

Subject Demographics and Neuropsychological Testing. Subjects were recruited from the University of California (Los Angeles) Memory Clinic at the Semel Institute for Neuroscience and Human Behavior to participate in an ongoing, comprehensive study of aging and dementia. Subjects performed a diagnostic evaluation that consisted of physical and neurological examinations, a medical history assessment, genotyping for apolipoprotein E (*APOE*), and neuropsychological testing. We excluded subjects on the basis of left-handedness, a history of neurological or psychiatric disorders, medication affecting cognition, alcohol or substance abuse, head trauma, epilepsy, arterial hypertension, or cardiovascular disease. Blood was drawn from each subject and genotyped for *APOE* (1).

The study included 30 *APOE*-4 noncarriers (average age, 63.8 ± 8.3 y; range, 45–76; 20 female; education, 16.7 ± 1.8 y; 21 with family history of dementia) and 25 *APOE*-4 carriers (average age, 60.8 ± 9.7 y; range, 43–78; 12 female; 21 3/4s, 4 4/4s; education, 17.5 ± 3.3 y; 16 with family history of dementia).

Subjects scored ≥27 on the mini-mental state examination (MMSE) with the exception of one subject who scored 26 but fell within the normal range on the remaining neuropsychological tests; analyses that excluded that subject found equivalent results. Forty-three of the 55 subjects were tested for subjective memory complaints, using the Memory Functioning Questionnaire (2). Scores were in the age-typical range and no significant between-group differences were found in frequency of forgetting (*APOE*-4, 157 ± 27; *APOE*-4 NC, 164 ±27), seriousness of forgetting (87 ± 25, 90 ±20), retrospective functioning (14.7 ± 4, 14.8 ±4.4), or mnemonics use (18.9 ± 8.6, 20.5 ± 8.4) (all $P > 0.2$).

The neuropsychological battery included (*i*) Wechsler memory scale, logical memory delayed recall portion (WMS LM delay); (*ii*) Buschke–Fuld selective reminding test (consistent long-term retrieval section, Buschke CLTR); (*iii*) Rey–Osterrith Complex Figure, delayed recall (Rey-O delay); (*iv*) Wechsler memory scale, verbal paired associations II (WMS VP); and (*v*) Wechsler Adult Intelligence Scale III digit span (WAIS digit span).

Diffusion Tensor Imaging (DTI) Preprocessing and Tractography. Scans were processed using programs from the FMRIB Software Library (FSL; www.fmrib.ox.ac.uk/fsl/). Diffusion tensors were then estimated at each voxel and fractional anisotropy (FA) images were created. Raw DTI images were first corrected for eddy current distortions using a 12-df affine registration to the first B0 volume.

Regional masks were transformed to each subject's diffusion space using a multistage registration process. First, the high-resolution structural image magnetization-prepared rapid gradient echo (MP-RAGE) was skull stripped using FSL's Brain Extraction Tool (BET). Next, the FA image was affine registered to the MP-RAGE using 12 degrees of freedom and a mutual information cost function using FSL's Linear Image Registration Tool (FLIRT). The MP-RAGE was then affine registered to the MNI152 brain using 12 df and a correlation ratio cost function. These two transformation matrices were multiplied and inverted to obtain the standard space-to-diffusion space transformation matrix.

The probability distribution of fiber direction(s) in each voxel was estimated using BEDPOSTX, configured to allow for up to two crossing fibers within each voxel (3). The dyads for the first and second vectors of diffusion direction within each voxel were used for tractography. Typically these dyads are used as the input to a probabilistic tractography program. However, probabilistic estimates of structural connectivity can be difficult to interpret when building a connectivity matrix. For this reason, we used these dyad vectors as the input for deterministic tractography, using the fiber assignment by continuous tracking (FACT) algorithm in Diffusion Toolkit (ref. 4 and http://trackvis.org/dtk). Whole brain tractography was carried out, propagating fibers from each voxel with a maximum turn angle of 50°. Fibers were smoothed using a spline filter and all fibers <5 mm were excluded. To control for false positives, any region–region pair with less than three connecting fibers had its connection strength set to 0. A fiber was defined as connecting two regions if one fiber endpoint lay within one region and the other endpoint lay within the other region.

Because the regions from the Harvard Oxford Atlas varied in volume (450–46,800 mm^3), the fiber counts had to be adjusted for the unequal number of seed voxels in each region. The fiber connectivity metric between two regions was therefore scaled by the mean of the two regions' volumes. This step had the additional benefit of correcting for individual variations in brain size with finer accuracy than can be achieved with a global correction for brain volume. Connectivity matrices resulted and ranged between 16.1% and 23.7% of regions connected. These individual variations in connection "density" had no significant relationship to any neuropsychological measure and decreased with age at nearly equal rates in the *APOE*-4 carriers and noncarriers.

Network Metrics. Given a weighted connectivity matrix, strength was calculated as the total weight of connections to a given node. To calculate cost, for each region–region connection the product of fiber count (i.e., connection weight, w_{ij}), average fiber length (l_{ij}), and average fiber FA (fa_{ij}) and was taken. The sum of all region–region costs was computed to derive the total network cost:

$$\sum w_{ij}\bar{l}_{ij}fa_{ij}.$$

For each node, the subgraph was defined as the subset of connections between the node and its first-degree neighbors. The clustering coefficient for a node was calculated as the ratio of the number of actual connections among the neighbors in the subgraph to the number of possible connections, scaled by the edge weights.

To calculate path lengths within the networks, the distance matrix was first defined. Distance was defined in two parts: First, the inverse of fiber density between two regions was calculated, with the rationale that a denser connection enables more communication and is equivalent to a shorter distance. Second, this distance was scaled by the actual average length of fibers connecting the regions. This distance scaling step allowed the quantification of network path lengths in terms of true physical distance. Shortest paths were determined between all pairs of nodes (e.g., node A and node B) in the network by finding the shortest distance between nodes A and B using Djikstra's algorithm, which finds all possible paths between A and B that travel through a unique, nonlooping set of other nodes. These paths are then sorted by distance, where distance is the product of the connection weight for each jump between nodes along the path and the anatomical distance between those nodes. Characteristic path length measured the average shortest path length in the network.

Small worldness for a network was calculated with respect to a set of equivalent "null" random networks that have the same sum of weights as the real network but have been randomly re-

wired. For each subject's structural network, we calculated 1,000 random networks for comparison. Normalized clustering coefficient was calculated as the ratio of the clustering coefficient from the real network to the average clustering coefficient of the 1,000 random networks. Normalized characteristic path length was calculated in the same fashion. Small worldness was quantified as the ratio of normalized clustering coefficient and normalized characteristic path length.

Graph Theory Formulas. Network measures were calculated with the Brain Connectivity Toolbox, which is based on formulas described elsewhere (5). Briefly, strength was calculated as $k_i = \sum w_{ij}$, where w_{ij} is the weight between nodes i and j.

Clustering coefficient was calculated as $C = \frac{1}{n}\sum \frac{\sum (w_{ij} w_{ih} w_{jh})^{1/3}}{k_i(k_i - 1)}$, where all w are weights and k is the number of nodes in the local, first-degree neighborhood.

Characteristic path length was calculated as $L = \frac{1}{n}\sum \frac{\sum d_{ij}}{n-1}$, where d_{ij} is the path weight between any nodes i and j in the network that pass through the specified node. The average of these path weights is the average path weight for the node. The average of the average path weights for each node is the characteristic path length.

Normalized clustering coefficient (CC) (λ) was calculated as $\lambda = \frac{\mathrm{CC}_{\mathrm{real}}}{\mathrm{CC}_{\mathrm{random}}}$, where $\mathrm{CC}_{\mathrm{random}}$ is the mean CC from the 1,000 random networks.

Normalized characteristic path length (CPL) (γ) was then $\gamma = \frac{\mathrm{CPL}_{\mathrm{real}}}{\mathrm{CPL}_{\mathrm{random}}}$, where again $\mathrm{CPL}_{\mathrm{random}}$ is the mean from 1,000 random networks.

Finally, small worldness (σ) was the ratio $\sigma = \frac{\lambda}{\gamma}$.

A small world network has no isolated nodes, $\lambda >> 1$, $\gamma \cong 1$, and $\sigma > 1.2$.

Graph Visualization. Network graphs were rendered using matplotlib (http://matplotlib.sourceforge.net) and networkX (http://networkx.lanl.gov).

Statistics. Three regression models were tested for mean clustering coefficient. Regression model 1, including only main effects, showed significant main effects of genotype ($P = 0.02$), sex ($P = 0.003$), and age ($P = 0.004$ or $P < 0.01$) on mean clustering coefficient and was significant overall [$f(49, 5) = 27.98$, $P = 2.79 \times 10^{-13}$]. Model 2, adding the age × genotype, showed a significant genotype × age interaction ($P = 0.04$) and was also significant overall [$f(48, 6) = 25.83$, $P = 1.82 \times 10^{-13}$]. Model 3, the model selected by stepwise regression, included genotype, sex, and genotype × age interaction. There was a significant age × genotype interaction ($P = 0.0005$) and the model was significant overall [$f(49, 5) = 31.17$, $P = 4.01 \times 10^{-14}$]. This model was the most accurate predictor of mean clustering coefficient.

The same three models were tested for mean cortical thickness, Rey-O delay, and WMS LM delay: model 1, mean cortical thickness [$f(50, 4) = 17.43$, $P = 5.16 \times 10^{-9}$], Rey-O delay [$f(51, 3) = 1.63$, $P = 0.19$], WMS LM delay [$f(51, 3) = 3.65$, $P = 0.02$]; model 2, mean cortical thickness [$f(49, 5) = 15.02$, $P = 6.18 \times 10^{-9}$], Rey-O delay [$f(50, 4) = 2.63$, $P = 0.044$], WMS LM delay [$f(50, 4) = 3$, $P = 0.03$]; and model 3, mean cortical thickness [$f(50, 4) = 19.06$, $P = 1.41 \times 10^{-9}$], Rey-O delay [$f(51, 3) = 3.58$, $P = 0.02$], WMS LM delay [$f(51, 3) = 3.89$, $P = 0.014$]. In every case, model 3 had the smallest P value.

Interpretability of the genotype × age interaction on regional clustering coefficient was also assessed by examining the partial correlation between age and regional clustering separately for *APOE*-4 carriers and noncarriers after controlling for the effect of sex, scanner, and total network cost.

1. Wenham PR, Price WH, Blandell G (1991) Apolipoprotein E genotyping by one-stage PCR. *Lancet* 337:1158–1159.
2. Gilewski MJ, Zelinski EM, Schaie KW (1990) The Memory Functioning Questionnaire for assessment of memory complaints in adulthood and old age. *Psychol Aging* 5:482–490.
3. Behrens TEJ, Berg HJ, Jbabdi S, Rushworth MFS, Woolrich MW (2007) Probabilistic diffusion tractography with multiple fibre orientations: What can we gain? *Neuroimage* 34:144–155.
4. Mori S, van Zijl PCM (2002) Fiber tracking: Principles and strategies - a technical review. *NMR Biomed* 15:468–480.
5. Rubinov M, Sporns O (2010) Complex network measures of brain connectivity: Uses and interpretations. *Neuroimage* 52:1059–1069.

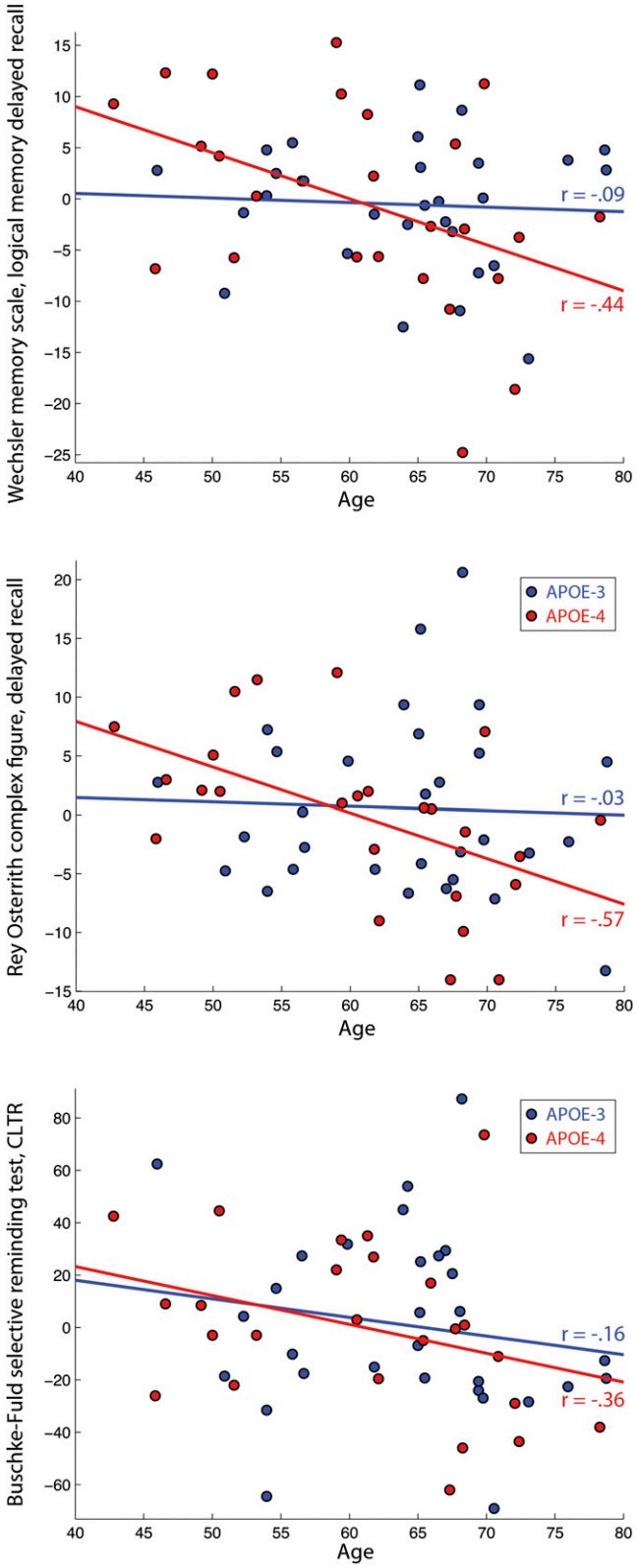

Fig. S1. Wechsler memory scale (logical memory delayed recall portion, WMS LM delay), Rey–Osterrith Complex Figure (delayed recall, Rey-O delay), and Buschke–Fuld selective reminding test (consistent long-term retrieval section, Buschke CLTR) residuals based on partial correlations with age plotted for *APOE*-4 noncarriers (*APOE*-3, blue) and *APOE*-4 carriers (red). Partial correlations controlled for sex. Both WMS LM delay and Rey-O delay had a significant interaction between *APOE* genotypes ($P < 0.05$).

Table S1. Top 12 regions with highest combined rank for strength, betweenness centrality, and regional short path length for *APOE*-4 noncarriers (*APOE*-4 NC) and *APOE*-4 carriers

APOE-4 NC	*APOE*-4
Left angular gyrus	Left insular cortex
Left precuneus	Right insular cortex
Left superior temporal gyrus (posterior)	Left posterior cingulate
Left intracalcarine cortex	Right cuneal cortex
Right supramarginal gyrus (posterior)	Left temporal pole
Left posterior cingulate	Right temporal pole
Left insular cortex	Right intracalcarine cortex
Left supramarginal gyrus (posterior)	Right posterior cingulate
Right insular cortex	Right precuneus
Left lateral occipital cortex (superior)	Left supramarginal gyrus (posterior)
Right intracalcarine cortex	Right frontal orbital cortex
Left middle temporal gyrus (temporooccipital)	Right lingual gyrus

Table S2. Regions that show a significant interaction in the selected regression model

Region	*APOE*-4 partial correlation with age, *r*	Associated *P* value	*APOE*-4 NC partial correlation with age, *r*	Associated *P* value	Comparison of correlation coefficients, *P* value
R precentral gyrus	−0.5	0.017	−0.2	0.33	0.03
R inferior temporal gyrus, anterior	−0.58	0.005	−0.13	0.52	0.01
L inferior temporal gyrus, posterior	−0.65	0.0009	0	0.97	0.005
L supramarginal gyrus, posterior	−0.54	0.009	−0.35	0.07	0.02
L subcallosal cortex	−0.54	0.009	−0.06	0.77	0.02
R anterior cingulate gyrus	−0.48	0.02	0.02	0.9	0.03
R precuneus cortex	−0.64	0.001	−0.13	0.53	0.006
L frontal orbital cortex	−0.5	0.02	−0.17	0.4	0.03

In all cases, the partial correlation of regional clustering and age is significantly negative for *APOE*-4 carriers ($P < 0.05$) and nonsignificant for *APOE*-4 noncarriers ($P > 0.05$), and the partial correlation coefficients are significantly different between groups ($P < 0.05$). L, left; R, right.